Atmospheric Environment 199 (2019) 224–232

Contents lists available at ScienceDirect

Atmospheric Environment

journal homepage: www.elsevier.com/locate/atmosenv

Investigation of levoglucosan decay in wood smoke smog-chamber experiments: The importance of aerosol loading, temperature, and vapor wall losses in interpreting results

Vikram Pratap[a], Qijing Bian[b], S. Aditya Kiran[a], Philip K. Hopke[a], Jeffrey R. Pierce[b], Shunsuke Nakao[a,*]

[a] Department of Chemical and Biomolecular Engineering, Clarkson University, Potsdam, NY, 13676, USA
[b] Department of Atmospheric Science, Colorado State University, Fort Collins, CO, 80523, USA

ARTICLE INFO

Keywords:
Markers
Levoglucosan
Biomass burning
Winter
Low-temperature

ABSTRACT

Levoglucosan has been extensively used as a molecular marker of biomass burning in source-apportionment studies over the last few decades. However, recent studies suggest that the atmospheric lifetime of levoglucosan may be in the order of only 1–2 days under summertime conditions relevant to prescribed/wildfires. Implications of levoglucosan reactivity to wintertime conditions, however, remain uncertain despite significant contributions of domestic wood combustion to wintertime air quality. This study presents smog chamber experiments to investigate levoglucosan decay during photo-oxidation of wood smoke over a temperature range between −8 and 10 °C.

Significant decay in particle wall-loss corrected levoglucosan is only observed around 10 °C in these experiments. Theoretical analysis shows that the apparent chemical lifetime of levoglucosan increases at lower temperatures as well as at higher organic aerosol mass concentrations as a result of smaller vapor fractions. The chemical lifetime of a molecular marker is commonly interpreted by a relationship between relative decay in particle wall-loss corrected marker concentrations versus integrated OH exposure. However, this relationship strongly depends on vapor wall-loss rates in addition to temperature, organic aerosol concentrations, and OH concentrations. Therefore, inferred lifetimes from a small set of experiments from a single chamber cannot easily be generalized for the full range of atmospheric smoke conditions.

1. Introduction

Domestic wood combustion is one of the major sources of atmospheric particulate matter (PM), especially in winter (Bergauff et al., 2009; Gorin et al., 2006). Reductions in emissions from industrial and transportation sources over the last few decades have resulted in increasing importance of wood combustion as a persistent air pollution source (Caseiro et al., 2009; Heal, 2014; Huang et al., 2014; Ofosu et al., 2013; Pandis et al., 2016). Many PM source-apportionment studies have used various molecular markers. Levoglucosan is one of the most widely used molecular markers for biomass burning (Hawthorne et al., 1988; Jaeckels et al., 2007; Oros and Simoneit, 2001; Pietrogrande et al., 2015; Schauer and Cass, 2000; Simoneit et al., 1999; Stone et al., 2009; Szidat et al., 2006; Wang et al., 2012). Although early studies assumed levoglucosan to be stable and non-volatile, recent studies suggested that levoglucosan is semi-volatile, and therefore gas-phase oxidation leads to short lifetimes of levoglucosan of approximately 1–2 days under room-temperature conditions (Hennigan et al., 2010; May et al., 2012). Therefore, source-apportionment studies using levoglucosan as a marker may underestimate the contribution of biomass burning to ambient aerosols under summertime conditions. In contrast, the winter reactivity of levoglucosan is expected to be significantly lower due to the reduced vapor pressure of levoglucosan (May et al., 2012) as well as low diffusivity within the condensed phase at low temperatures (Arangio et al., 2015). Despite the widespread use of levoglucosan in PM source-apportionment studies in winter, to our knowledge, only one recent study (Bertrand et al., 2018a) evaluated the evolution of levoglucosan in laboratory experiments at low temperature. Bertrand et al. (2018a, b) concluded that partitioning and vapor wall loss play a predominant role in the apparent decay of semi-volatile marker species while the reactivity with OH has a minor effect in their smog chamber at −2 °C. However, the implications of their findings to other conditions, especially temperature, remain unclear. In addition, the winter reactivity of levoglucosan may have an implication to

* Corresponding author. Department of Chemical and Biomolecular Engineering Clarkson University, 8 Clarkson Ave, Potsdam, NY, 13699, USA.
E-mail address: snakao@clarkson.edu (S. Nakao).

https://doi.org/10.1016/j.atmosenv.2018.11.020
Received 1 April 2018; Received in revised form 23 October 2018; Accepted 11 November 2018
Available online 14 November 2018
1352-2310/

geochemical studies exploring the presence of biomass burning markers in ice cores to estimate the wildfire events several hundred years ago (Kawamura et al., 2012). Here, we present smog chamber experiments to systematically evaluate the reactivity of biomass burning markers in -8 °C to +10 °C temperature range.

2. Materials and method

2.1. Experimental setup

The experimental setup was installed in/on an INTERMODAL shipping container. The experiments were performed in a 6 m^3 outdoor pillow shaped Teflon smog chamber resting on the roof of the shipping container and subject to ambient conditions. We used 64 Eiko 15 W UV lamps and installed them on the sides of the chamber. The chamber is surrounded by a wooden structure on top and three sides and covered by a tarp to protect the chamber from the outer elements. The tarp also blocks sunlight to minimize variation in the light source. Schematic of the experimental setup is shown in Fig. 1. Temperature studied in these experiments was in the range of -8 °C to +10 °C. The wood stove used is a Morso model no. 1125 built in Denmark in 1980s. We used local seasoned softwood (Tamarack) and hardwood (Maple). Typically, four wood logs were used in each experiment. Wood logs were usually 30–40 cm long and triangular or trapezoidal in cross-section. All the experiments were performed during the flaming stage of the burn where the Modified Combustion Efficiency (MCE = $CO_2/(CO_2+CO)$ (Yokelson et al., 1996),) is usually more than 90%. Table 1 lists the details of the fuels and fire conditions in each experiment.

The emission sampling location was on the chimney at an approximately 60 cm above the fire area. An ejector dilutor (Air-Vac, TD260HSS) was used to inject diluted smoke into the chamber. The line from the chimney to the ejector dilutor was ~60 cm copper tubing (1/4″ OD). The tubing temperature was not actively controlled. Since fresh smoke was continuously sampled through the tubing over 30 min prior to injection into the chamber, semi-volatile vapors in smoke were assumed to be in equilibrium with the tubing surface. The dilution air was generated by cleaning the compressed air (oil-free compressor) using a HEPA filter, 13X molecular sieves, and silica gel. The dilution ratio was determined using the CO measurements of the raw wood smoke and the diluted smoke, with an average value of approximately 250. The humidity of the dilution air was kept below 5%. Hydroxyl radicals (OH) were generated by photo-oxidation of nitrous acid (HONO). HONO was generated by mixing sulfuric acid (H_2SO_4) and sodium nitrite ($NaNO_2$) and flushing the headspace with the dilution air (Taira and Kanda, 1990). 150 ml of 3 mM $NaNO_2$ solution was added to 50 ml of 10 mM H_2SO_4 solution. The mixture was heated once to 33 °C, and then the heating was stopped during the entire HONO injection. The chamber was also doped with an approximately 10 µl of methanol and ethanol mixture (50:50 vol/vol) after the wood smoke injection. The initial concentrations of methanol and ethanol were around 500 ppb and 350 ppb, respectively. For methanol and ethanol sampling, 400 ml SS ENTECH canisters MC400L were used. First order reactive losses of methanol and ethanol over the period of the experiment was used to estimate the OH concentration in the chamber. A 47 mm filter sample collection assembly comprised of two lines: one with Teflon and quartz in series, while the other with quartz only. The filter assembly used was Advantec MFS, Inc. LS47 gas line holder 304SS. The Teflon and quartz filters used for collecting samples were from Pall Corporation. The nominal flow rate for filter sample collection was 15 lpm for each line maintained using 15 lpm critical orifice supplied by O'Keefe Controls Co. Three HONO injections were typically performed during the experiment prior to and between sampling, which led to four filter and canister samples. The filter samples were stored in a freezer until analysis.

2.2. Instrumentation

The moisture of the wood logs was measured using a Delmhorst J-2000 as per the technique described in Smith et al. (2014). Thermo Electron Corporation Model 42i and 49i were used to measure nitrogen oxides (NO_x) and ozone (O_3) respectively. An IMR 5000 gaseous emissions monitor was used to measure NO_x, CO, CO_2, and O_2. The temperature and

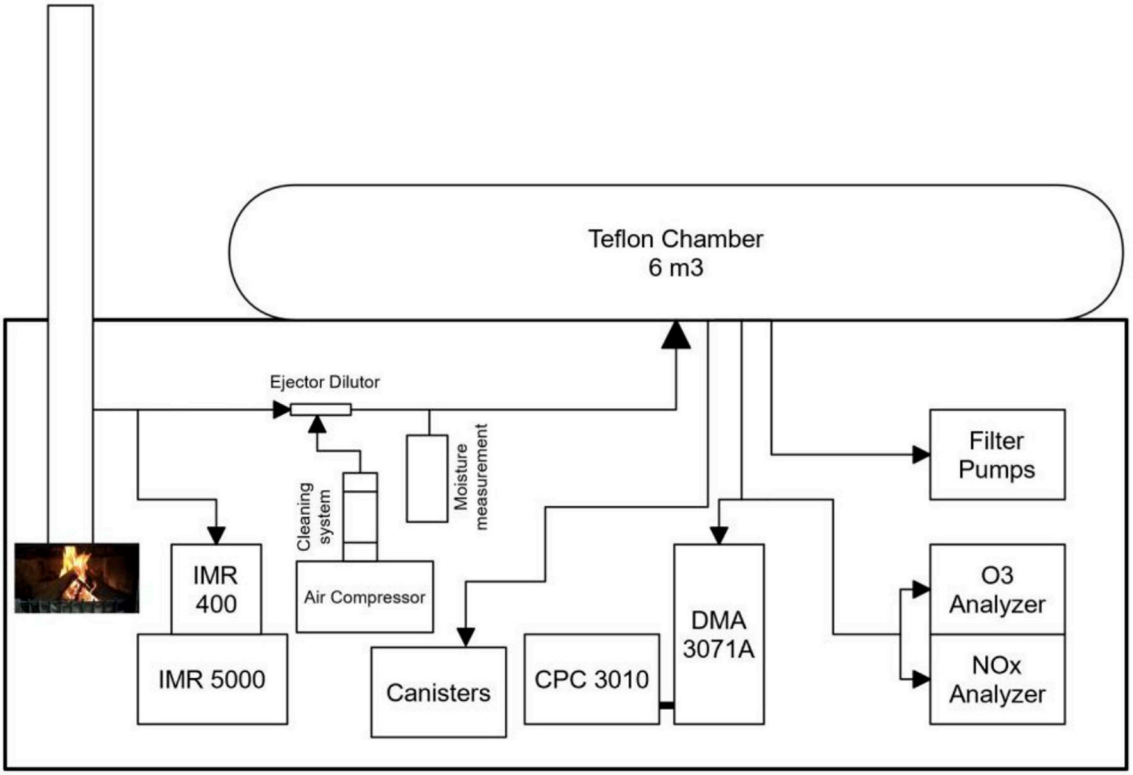

Fig. 1. Schematic of the experimental setup.

Table 1
Experimental conditions.

Exp.	Wood type	Average wood moisture (%)	Experiment temperature (°C)	Relative humidity (%)	MCE	Fresh smoke OA (μg m^{-3})[a]	Levoglucosan fraction in fresh smoke OA	Mean OH (molec cm^{-3})
1	Tamarack	12.3%	5	13.5–49.8	0.92	102	0.36	1.6×10^{7}[c,d]
2	Tamarack	12.0%	−6	1.8–15.7	0.89	124	0.23	9.1×10^{6}[c,d]
3	Maple	16.3%	10	18.9–40.1	0.90	278	0.18	3.5×10^{7}[c]
4	Maple	12.6%	−8	32.9–63.1	0.91	403	0.19	1.5×10^{7}[c]
5	Maple	14.4%	−3	52.6–78.0	0.91	215	0.19	2.0×10^{7}[b]
6	Maple	12.1%	3	30.0–80.7	0.92	224	0.11	2.8×10^{7}[b]

[a] Assuming OM/OC = 1.6.
[b] Determined by methanol/ethanol decay.
[c] Estimated by temperature-OH relationship.
[d] Corrected for a different amount of $NaNO_2$.

humidity of the content of the chamber were measured using a Rotronic HC2A-S3 humidity probe. The ambient temperature was measured using a LabJack Digit-TLH temperature logger. The temperature of the UV lamp panels was recorded using a LabJack EI-1034 thermocouple. The temperature of the sheath flow in a scanning mobility particle sizer (SMPS, TSI 3071) was recorded using a LabJack EI-1034 thermocouple to confirm there was no considerable difference between the ambient and sheath air temperature. During the smoke injection, the diluted smoke was analyzed using a LASCAR EL-USB-CO carbon monoxide logger. An SMPS system comprised of a differential mobility analyzer (DMA-3071A, TSI) and a condensation particle counter (CPC-3010, TSI) was used for particle size-distribution measurement. The canisters were analyzed using a Thermo Trace gas chromatograph (GC) Ultra and DSQ-II MS, a single quadrupole MS (Mass Spectrometer) using electron impact (EI) ionization. The column used was Restek Rxi- 5 ms that was 30 m long, 0.25 mm I.D and 0.25 μm film thickness. The sample was fed to it through the Markes Unity plus CIA system. The Markes system pulls 10 ml of gas sample from a canister, concentrates it and sends to the GC. Helium was used as the carrier gas and introduced to the GC through the Markes system such that a pressure of 15 psi was maintained in the GC column. The temperature gradient used was 40 °C for 2 min and then a ramp of 5 °C per minutes to 80 °C.

Levoglucosan in filter samples was analyzed using an Agilent 7890B GC coupled to a 5977A MS detector (single quadrupole GC using EI technique). The column used was a Restek Rxi- 5 ms 30 m long, 0.25 mm I.D and 0.25 μm film thickness. Simultaneous full scan and selected ion monitoring (SIM) scan were performed with each sample. Helium was used as a carrier gas with a constant flow of 1 ml min^{-1}. The oven was preheated to 90 °C, and then heated to 300 °C at 15 °C min^{-1} ramp ate. The temperature was held at 300 °C for 6 min to make the total run of 20 min. The quartz filters were analyzed for elemental carbon and organic carbon (EC/OC) using the IMPROVE_A method in a DRI model 2001.

2.3. Experiment protocol

The fire was started using paper and kindling. The smoke was injected into the chamber only after all kindling were burnt, and the wood was in the flaming phase. After 15 min of mixing since the injection of wood smoke, the first set of canister samples and filter samples were collected. Initial OA concentration in the chamber ranged between 102 and 403 μg m^{-3} (Table 1). Then the UV lamps were switched on, and the headspace of the aqueous solution of $NaNO_2$ and H_2SO_4 was continuously flushed with ~2LPM of purified air typically for an hour for HONO injection, which results in negligible dilution in the chamber. The second set of samples was collected immediately after the first HONO injection assuming the majority of HONO injected is well mixed after an hour of continuous HONO injection. Just after the second sample, second HONO injection was started and continued until the third sample. This process was repeated for one more sample set. After each experiment, the chamber was cleaned by adding HONO with the lights on and 3–4 flush cycles to reach a target particle concentration below 1×10^{-2} μg m^{-3}. Background experiments were performed to make sure the background PM concentrations were within the desired limit (typically < 3 μg m^3). A summary of experimental conditions is shown in Table 1.

The Teflon filter samples were weighed using Mettler-Toledo Sartorius microbalance model MC5 and Anti-Static bar with U-shaped electrode ionizer to measure the particle mass concentration in the chamber. Then the organics on the filter was extracted in 50 ml of acetonitrile by sonicating for 20 min. The extract was then concentrated 100 times using N_2 as the flush gas in a concentrator setup (Organomation Associates Inc. Model 11106). Levoglucosan was derivatized using *N*-Trimethylsilyl-*N*-methyl trifluoroacetamide (MSFTA). To a 35-μl sample, 35 μl of MSFTA was added and kept in an oven at 60 °C for 30 min. A sample of 1 μl is injected through a splitless column heated at 250 °C. To account for the extraction efficiency, the filter samples were spiked with methyl α-D-xylopyranoside (MXP), which was used as an internal standard. Levoglucosan and MXP were both detected at m/z of 204.

2.4. Data analysis

The concentrations from the filter analysis were converted to the mass concentration per volume of sampled air (μg m^{-3}). The concentrations of levoglucosan were normalized by the EC mass concentration to correct for particle wall loss as described in previous studies (Hennigan et al., 2010; Hildebrandt et al., 2009; Weitkamp et al., 2007). The equation used and the uncertainty is discussed in the supplemental information (1.1 Particle wall-loss corrected levoglucosan). Although particle number concentrations could also be used for particle wall-loss correction (Carter et al., 2005), the high initial particle number concentration in the chamber (typically > 100,000 particles cm^{-3}) leads to significant coagulation, which can complicate particle wall-loss correction (Nah et al., 2017). Therefore, the EC-based correction (Hennigan et al., 2010) was applied to the experimental data. Particle number-size distributions were used to constrain simulated particle wall loss as discussed in the model description. All particle species at a given size undergo the same wall loss rate. The wall-loss corrected levoglucosan concentrations were further normalized by the initial value. Since the time between the first filter sample and switching on of the UV lamps (t_0) varied among experiments, the initial values of levoglucosan and EC were calculated by correcting for particle wall-loss between t_0 and the first sample. The OH concentrations in Experiment 5, 6, and another higher temperature experiment (not included in Table 1) were determined based on the first-order decay of ethanol and methanol used as OH tracers in the chamber. In experiments where ethanol and methanol samples were not available (Experiment 1, 2, 3, and 4), OH concentrations were estimated by fitting the observed relationship between OH concentration and temperature into a polynomial, where lower temperature results in weaker irradiance of the blacklights (Platt et al., 2013) and thus lower the HONO photolysis rate and the OH concentration. In Experiment 1 and 2, HONO synthesis was carried out using 80 ml of $NaNO_2$ solution instead of 150 mL and hence estimated OH

concentrations were scaled assuming linearity between HONO and $NaNO_2$ concentration (Taira and Kanda, 1990). The OH concentrations varied in the range of $9.1 \times 10^6 - 3.5 \times 10^7$ molecules cm^{-3}.

2.5. Model description

This study uses an aerosol-microphysical model to evaluate the potential impacts of temperature, OH concentration, SOA formation, particle wall-loss, and vapor wall-loss on the interpretation of levoglucosan decay within a smog chamber. The details of the model are discussed elsewhere (Bian et al., 2017, 2015). Briefly, Bian et al. (2015) used simulations of particles in dark (slow oxidation) wood-smoke smog-chamber experiments to explore the role of the particle and vapor wall-losses in the evolving chamber aerosol, and both wall-loss processes were found to reduce the suspended aerosol mass. Bian et al. (2017) extended this work to explore wood-smoke smog-chamber experiments with lights and oxidation, and they included gas-phase oxidation and SOA formation within their simulations and explored the interplay between wall-losses and oxidation. In Bian et al. (2015, 2017) and in this work, the TwO-Moment Aerosol Sectional (TOMAS) microphysics model is coupled to the organic Volatility Basis Set (VBS) (TOMAS-VBS). TOMAS-VBS includes 36 size sections spanning dry diameters from 3 nm to 10 μm, and 15 organic volatility bins spanning saturation vapor concentrations of 10^{-3} to 10^{11} μg m^{-3} at 25 °C, respectively. Two sets of turbulence rate (k_e, s^{-1}) are retrieved by applying aerosol parameter estimation (APE) model (Pierce et al., 2008) on the dark period before photo-oxidation experiment for a warm (5 °C) and a cold experiment (−3 °C), respectively. These turbulence rates are used to estimate particle wall-loss rates and reversible vapor-wall-loss rate coefficients as described in Bian et al. (2015, 2017). The estimated k_e values are 0.3 s^{-1} at 5 °C and 1.0 s^{-1} at −3 °C, and the estimated size-independent particle wall-loss coefficients ($k_{w,p0}$ s^{-1}) are 7.4×10^{-5} s^{-1} (see Pierce et al., 2008 for detailed descriptions of these variables) These values are within the range of the previous observation by Bian et al. (2015). The equivalent organic mass concentration of the wall (C_w) is estimated as a function of C^* using the parameterization developed in Krechmer et al. (2016). Levoglucosan is independently added into the VBS to monitor its oxidation separately. The initial levoglucosan concentration is assumed to be 10% of the total organic matter (particle + vapor) in the model, which corresponds to approximately 20–25% of OA for the initial OA mass fractions. The modeled levoglucosan OA fraction (20–25%) is within the range observed in this study (Table 1) and in previous studies (e.g., 14.6%, Hennigan et al. (2010); 14–48%, Bertrand et al. (2018a)). The OH oxidation rate constant for levoglucosan was set to be 2×10^{-11} cm^3 $molecules^{-1}$ s^{-1} (May et al., 2012). The saturation vapor concentration of levoglucosan at 298 K was assumed to be 13 μg m^{-3} with an enthalpy of vaporization of 101 kJ mol^{-1} (May et al., 2012). The SOA chemistry in this study for the non-levoglucosan organics adopts the "lower-bound" mechanism of Bian et al. (2017) where each reaction with OH drops the volatility of the organics by a factor of 100. The formation yield of the organic-OH reaction products is set to 0.4 in order to reproduce the relatively low OA mass enhancements observed in this study (Fig. S2), and we evaluate this assumption in the supplemental information (2. Model sensitivity to the formation yield of low volatile products). We include no aerosol-phase or heterogeneous reactions in the model. The reaction rates are saturation-concentration dependent using the mathematical relationship derived by Jathar et al. (2014) for alkanes. We test the simulations with OH concentration of 3×10^7, 1×10^7 molecules cm^{-3}, which approximately correspond to the range of OH concentrations in the chamber, as well as 0 molecules cm^{-3}. The initial aerosol size distribution is fixed across different simulations to allow direct comparisons between different temperature and OH conditions. Therefore, experimental results are not directly used as model inputs except for slightly adjusting the wall-loss parameters and the formation yield of low volatile products.

3. Results and discussion

Experimental conditions are summarized in Table 1. Fig. 2 shows the evolution of particle wall-loss corrected levoglucosan concentrations normalized by the initial values. The estimation of experimental uncertainties (represented as error bars in Fig. 2) is discussed in the supplementary information. The majority of the results indicate no significant change in the normalized levoglucosan concentration. Only the experiment at ~ +10 °C (Experiment 3) showed significant decay. Although the results may indicate temperature-dependence of the apparent decay of levoglucosan, it remains uncertain due to the large variability. In addition, it is unclear if the significant levoglucosan decay between ~ −8 to +10 °C is due to chemical loss (e.g., reaction with OH) or physical loss due to vapor wall-loss in the Teflon chamber. In principle, controlled dark chamber experiments performed at identical temperatures and organic mass concentrations using a dual-chamber approach would provide clear insights into the effects of chemical perturbations (Tkacik et al., 2017).

In order to evaluate the potential role of chemical loss, a simple calculation is performed here that assumes the total aerosol loading stays fixed and ignores vapor and particulate wall loss. The purpose of the calculation is to evaluate the approximate effects of the entire temperature and organic mass concentration range. More detailed simulations based on TOMAS-VBS are used to provide further details on select conditions.

May et al. (2012) investigated the effects of gas-particle partitioning and chemical oxidation on semivolatile marker lifetime using the following equations:

$$\frac{dC_{p,i}}{dt} = -CS_p(X_{m,i}KeC_i^* - C_{g,i}) - k_p[OH]C_{p,i} \quad (1)$$

$$\frac{dC_{g,i}}{dt} = CS_p(X_{m,i}KeC_i^* - C_{g,i}) - k_g[OH]C_{g,i} \quad (2)$$

$$CS_p = 2\pi N_t d_p DF \quad (3)$$

where $C_{p,i}$ is the particle-phase concentration of i, $C_{g,i}$ is the gas-phase concentration of i, CS_p is the aerosol condensation sink, $X_{m,i}$ is the mass fraction of species i in the condensed organic matter ($=C_{p,i}/C_{OA}$), Ke is the Kelvin effect, C_i* is the saturation concentration of i, k_p is the heterogeneous oxidation rate constant, k_g is the gas-phase oxidation rate constant, N_t is the total aerosol number concentration, d_p is the particle diameter, D is the diffusion coefficient for the organic vapor, and F is the Fuchs correction factor. For simplicity, neglecting the heterogeneous reactions ($k_p \approx 0$), the Kelvin effect ($Ke \approx 1$), and assuming that the gas-phase levoglucosan is in a steady-state ($\frac{dC_{g,i}}{dt} \approx 0$), Eqs. (1) and (2) is reduced to

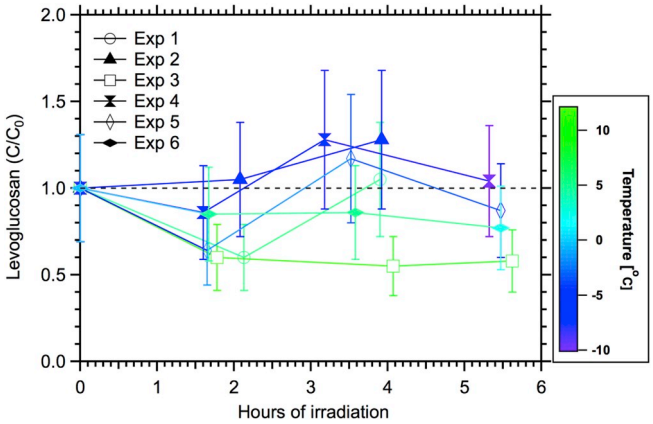

Fig. 2. Experimental results of levoglucosan decay at different temperatures. Levoglucosan concentrations were normalized by EC to correct for the particle wall-loss.

$$\frac{dC_{p,i}}{dt} \approx -k_g[OH]C_{g,i}. \quad (4)$$

Introducing the gas-particle partitioning coefficient (Donahue et al., 2006),

$$\xi_i = \left(1 + \frac{C_i^*(T)}{C_{OA}}\right)^{-1} = \left(1 + \frac{C_{g,i}}{C_{p,i}}\right)^{-1}, \quad (5)$$

where ξ_i is the partition coefficient of i representing the fraction of i found in the condensed phase. Using Eqs. (4) and (5),

$$\frac{dC_{p,i}}{dt} = -k_g[OH]\frac{1-\xi_i}{\xi_i}C_{p,i}. \quad (6)$$

When ξ_i is constant, *i.e.*, constant temperature, C_{OA}, and activity coefficient, integration of Eq. (6) yields

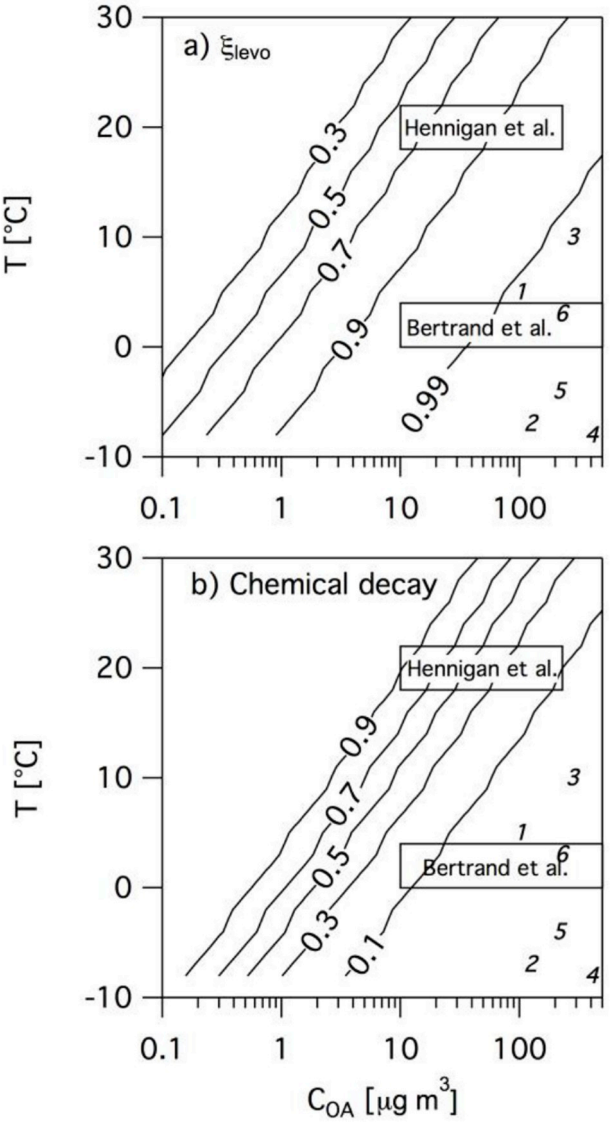

Fig. 3. (a) Estimated gas-particle partition coefficient (the fraction of levoglucosan mass in the particle phase at equilibrium) and (b) chemical decay fraction of levoglucosan as a function of temperature and organic aerosol mass concentration. The calculation in (b) used Eq. (7) and assumed $k_g = 2 \times 10^{-11}$ cm^3 molecule^{-1} s^{-1}, [OH] = 1×10^7 molecules cm^{-3}, and t = 5 h. The temperature and OA concentration ranges used in Hennigan et al. (2010) and Bertrand et al. (2018b) are shown as boxes. The initial conditions of six experiments in this study are shown as numbers (1–6).

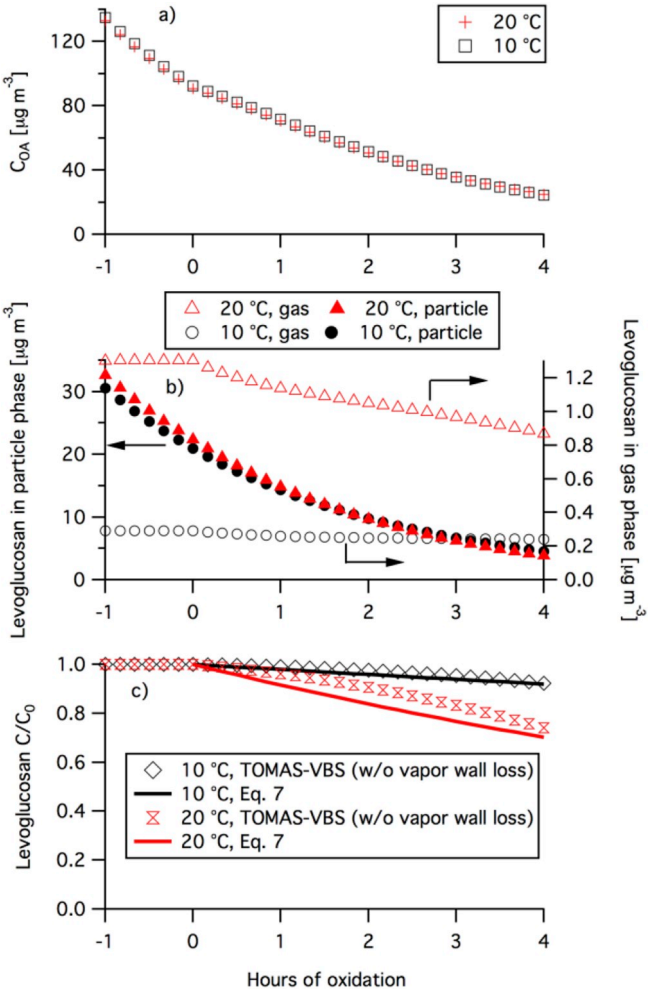

Fig. 4. a) Simulated time evolutions of organic aerosol mass concentrations using the TOMAS-VBS model. b) Simulated time evolution of levoglucosan concentrations in the gas and particle phase using the TOMAS-VBS model. c) Simulated time evolution of particle wall-loss corrected levoglucosan decay using the TOMAS-VBS model and Eq. (7). All calculations assume no vapor wall-loss and OH = 1×10^7 molecule cm^{-3}.

$$\frac{C_{p,i}}{C_{p,i}^0} = exp\left(-k_g[OH]\frac{1-\xi_i}{\xi_i}t\right). \quad (7)$$

The temperature dependence of C_i^* (and ξ_i) is calculated by the Clausius-Clapeyron equation (Epstein et al., 2010):

$$R\ln\left[\left(\frac{T_2}{T_{ref}}\right)\left(\frac{C^*(T_2)}{C^*(T_{ref})}\right)\right] = \Delta H^{VAP}\left(\frac{1}{T_{ref}} - \frac{1}{T_2}\right), \quad (8)$$

where R is the gas constant, T_{ref} is the reference temperature, T_2 is the new temperature, and ΔH^{VAP} is the enthalpy of vaporization.

Using Eqs. (5), (7) and (8), one can estimate the approximate extent of the chemical loss, $1 - \frac{C_{p,i}}{C_{p,i}^0}$, of a semivolatile marker as a function of temperature and C_{OA} (Fig. 3). The calculation assumes an OH concentration of 1×10^7 molecule cm^{-3} and 5 h of oxidation as a plausible chamber condition with elevated OH. A lower OH concentrations would result in a smaller chemical decay fraction in Fig. 3b. Fig. 3a shows that a significant fraction of levoglucosan exists in the gas-phase under the conditions of Hennigan et al. (2010), whereas the fraction is only ~1% or less under the conditions of Bertrand et al. (2018b) and this study. As a result, the estimated chemical decay via gas-phase oxidation is generally < 10% in this study. Since the experimental uncertainty of the particle wall-loss corrected levoglucosan in this study is approximately 30% (Supplementary

information), the effect of chemistry is expected to be within the experimental uncertainty and thus, cannot be resolved. Therefore, the temperature effects in Fig. 2 are likely to be due to physical vapor wall-loss, rather than chemical reaction loss. The TOMAS-VBS model also shows that the majority of levoglucosan decay at 10 °C is due to the vapor wall-loss (Fig. 6a) as discussed later in this section. The minor role of chemical loss is consistent with Bertrand et al. (2018b) in which the partitioning and vapor wall-loss played a predominant role in the depletion of particle-phase levoglucosan in their experimental conditions. However, it should be noted that chemical loss can play a significant role (~30%) even at temperature ~0 °C if the experiments can be carried out at C_{OA} ~ 1–10 μg m^{-3} (Fig. 3b); the challenge is the quantification of levoglucosan at such low concentrations. The potential effects of organic mass concentrations on apparent levoglucosan lifetime has not been considered in previous studies (Hennigan et al., 2010; May et al., 2012; Bertrand et al., 2018a). For instance, if wood smoke dilutes into a background with total OA < 10 μg m^{-3}, the lifetime of levoglucosan would be shorter than temperature alone could explain. Alternatively, high OA concentrations in wintertime pollution events would increase the lifetime of levoglucosan.

Despite the number of approximations made in the derivation of Eq. (7), the simplified estimates using Eq. (7) reasonably agree with the TOMAS-VBS model without vapor wall-loss. Fig. 4 shows time-series of organic aerosol concentrations, levoglucosan concentrations in the gas and particle-phase, and the normalized, particle wall-loss corrected levoglucosan simulated by the TOMAS-VBS model at 10 °C and 20 °C with OH concentration of 1 × 10^7 molecule cm^{-3}. The gas-phase levoglucosan concentrations at 10 °C are nearly constant (Fig. 4b), showing that the steady-state approximation made in Eq. (4) is reasonable, although some decrease is observed at 20 °C. Levoglucosan decays are calculated by Eq. (7) using the average value of C_{OA} during oxidation (54 μg m^{-3}). Eq. (7) gives a lower C/C$_0$ than TOMAS-VBS because TOMAS-VBS simulates the decreasing OA concentrations (mostly due to particle wall losses) with time, and initially TOMAS-VBS has a higher concentration than Eq. (7). Therefore, Eq. (7) initially overestimates the gas-phase oxidation compared to TOMAS-VBS (but underestimates at the end when TOMAS-VBS predicts less OA than Eq. (7)). Since these calculations neglect vapor wall-loss, the chemical loss estimated by Eq. (7) is the upper limit with respect to gas-phase oxidation.

Next, we performed simulations using the TOMAS-VBS model to illustrate the effects of vapor-particle-wall partitioning in the observed levoglucosan decay in the smog chamber. Again, due to the large experimental uncertainties, the objective of the simulation is not to obtain the best fit with the experiments in the wide parameter space, but rather to demonstrate the implications of vapor wall-loss in interpretation of experimental results using plausible parameters similar to the ones used in Bian et al. (2017). Fig. 5 shows the model time series for all organics and levoglucosan in each phase for two different temperatures and with and without OH oxidation. Fig. 5a and (b) shows the results

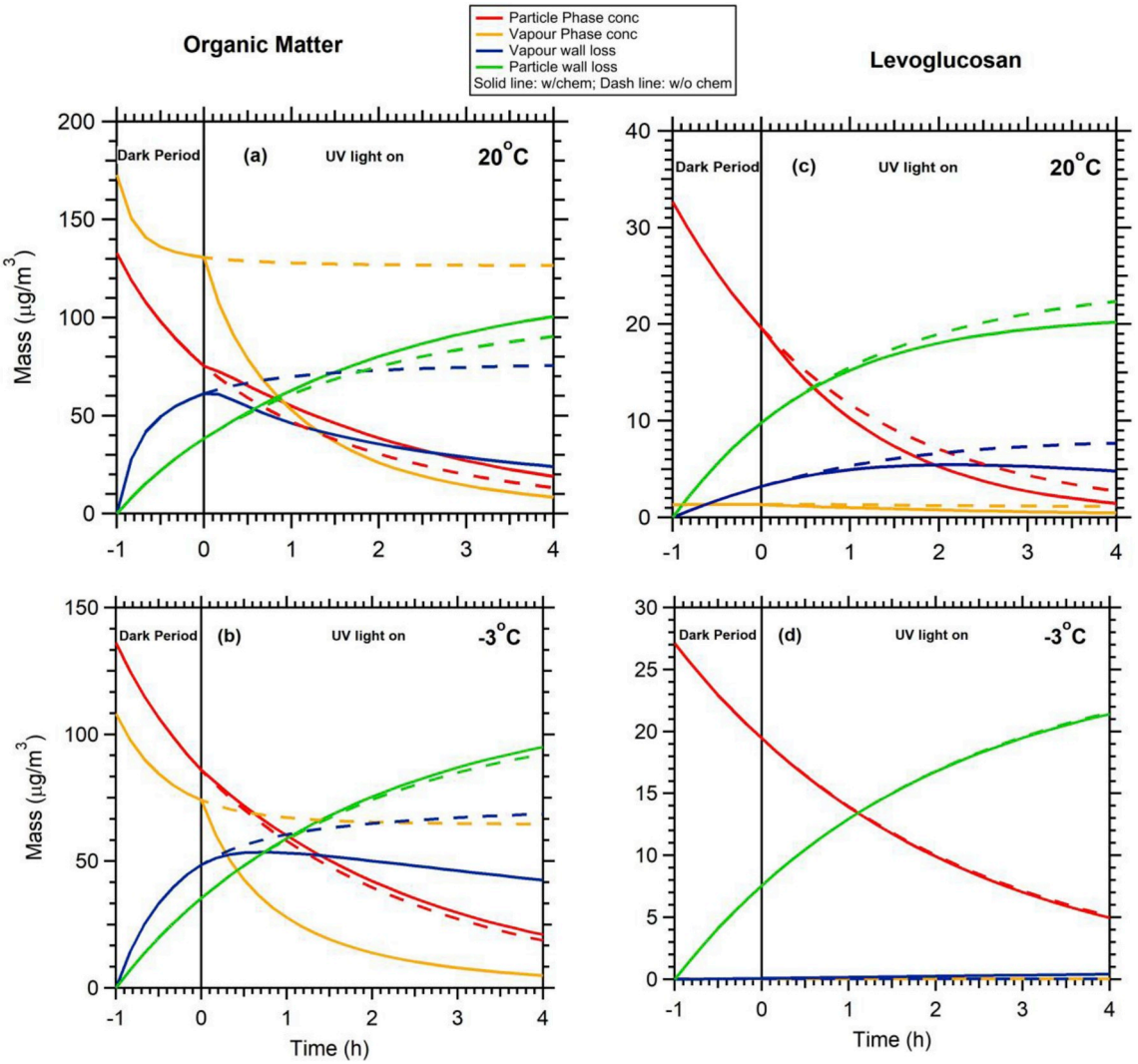

Fig. 5. Simulated time evolution of organic mass (OM) in different phases in TOMAS-VBS model with particle and vapor wall-loss on. Solid lines show results for an OH concentration of 3 × 10^7 molecules cm^{-3}, and dashed lines at zero OH. (a) and (b) are the results for total organics, and (c) and (d) are of levoglucosan.

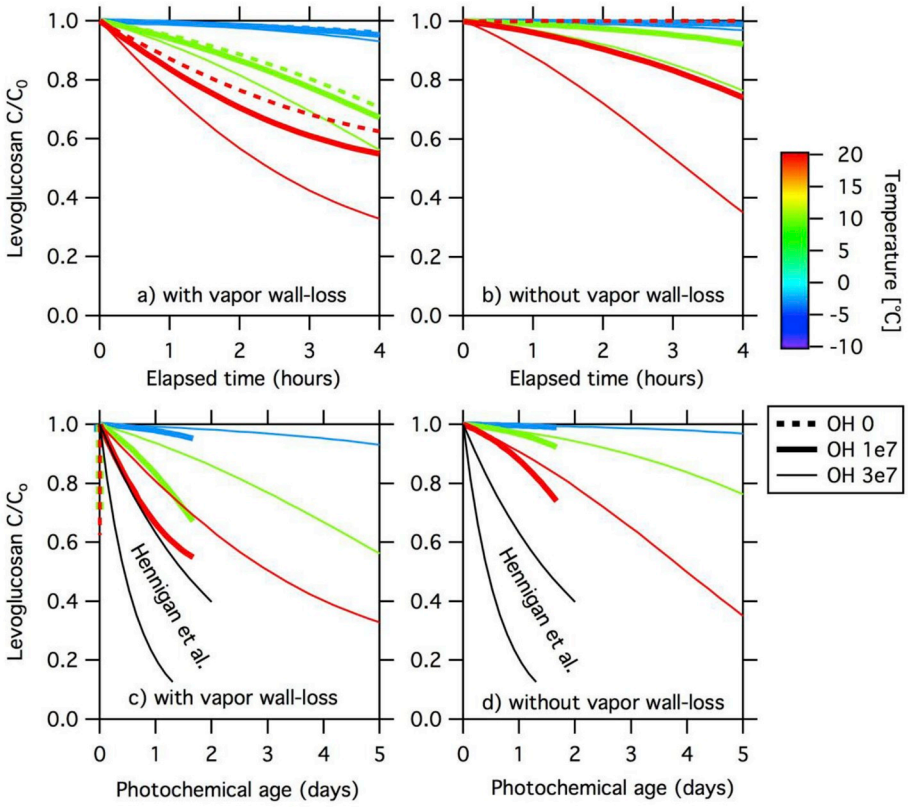

Fig. 6. Simulated decay of particle wall-loss corrected levoglucosan at different temperature (−3, 10, and 20 °C) and OH concentrations (0, dashed lines; 1×10^7, thick solid lines; and 3×10^7 molecule cm^{-3}, thin solid lines) using the TOMAS-VBS model. The initial C_{OA} is ~130 μg m^{-3}. The elapsed time (a, b) is equivalent to the experimental time in a smog chamber. The photochemical age (c, d) is equivalent to the integrated OH exposure assuming OH = 1×10^6 molecule cm^{-3} as the ambient OH concentration. Also shown are the upper and lower bound observed by Hennigan et al. (2010). The vapor wall-loss is turned off in b and d.

for organic matter in particle-phase, gas-phase, and on the wall through particle- and vapor-phase wall-losses at 20 °C and −3 °C, respectively. The vapor wall-loss is higher when no OH is present indicating that higher SOA formation shifts the gas-particle partitioning toward the particle phase and thus reduces vapor wall-loss. The impact of OH concentration on the particle phase concentrations is larger at 20 °C due to a higher fraction of initial organics being in the vapor phase at higher temperatures due to higher temperatures increasing volatility. Thus, at higher temperatures, the model has more SOA precursor vapors. Fig. 5c and (d) illustrates the same parameters for levoglucosan exclusively. There is little apparent difference in the predicted levoglucosan concentrations between with and without OH at −3 °C. This is because more than 99.8% of initially suspended levoglucosan (vapor + particle) remains in the particle phase (compared to just 92% at 20 °C), and therefore the reactive losses of levoglucosan by OH in the gas-phase is negligible. Vapor wall-loss of levoglucosan is significant at 20 °C, consistent with recent studies on the significance of vapor wall-loss (Matsunaga and Ziemann, 2010; McVay et al., 2014; Trump et al., 2016), but negligible at −3 °C due to the low concentrations of levoglucosan vapors at this low temperature. Although Hennigan et al. (2010) observed a modest decrease in levoglucosan in the dark experiment, ~10% over 3 h, they concluded that the reason for the decay was unknown; we suspect the decay was due to the vapor wall-loss.

Previous studies presented results of levoglucosan decay in terms of integrated OH exposure, or photochemical age (Bertrand et al., 2018a; Hennigan et al., 2010). Fig. 6 shows simulation results of particle wall-loss corrected levoglucosan decay in terms of elapsed time and photochemical age (assuming ambient OH = 1×10^6 molecule cm^{-3}) using the TOMAS-VBS model. Each case has the same initial C_{OA} of ~130 μg m^{-3}. The decay of levoglucosan at zero OH is due to vapor wall-loss based on the parameters used in Bian et al. (2015) (Fig. 6a). When vapor wall-loss is turned off, there is no decay in the particle wall-loss corrected levoglucosan at zero OH (Fig. 6b). When there is significant vapor wall-loss at zero OH, the trend appears as vertical lines in terms of photochemical age since the integrated OH exposure is zero (Fig. 6c). Comparisons between the levoglucosan estimates when vapor wall loss is on (Fig. 6a,c) to estimates when vapor wall loss is off (Fig. 6b,d) show that a substantial fraction of the observed levoglucosan decay in these experiments may be because of vapor wall losses, even ~50% of the decay for the highest OH concentrations. Thus, the decay trend of levoglucosan in smog-chamber oxidation experiments depends on a number of experimental conditions: C_{OA}, OH concentration, temperature, and vapor wall-loss rate. Additionally, SOA formation adds to C_{OA} and will affect levoglucosan decay (Fig. 5). Therefore, inferred lifetimes from a small set of experimental conditions cannot be generalized for the full range of atmospheric smoke conditions. The supplementary material includes discussion on the sensitivity of model simulations to assumed formation yields of less volatile species.

4. Conclusions

This study performed smog chamber experiments to investigate the evolution of levoglucosan over a temperature range between −8 and 10 °C. Only the experiment at around 10 °C showed significant decay of levoglucosan, suggesting that levoglucosan is relatively stable as a marker species at low temperatures. Theoretical analysis showed that both temperature and OA mass concentrations affect the chemical decay of levoglucosan by shifting gas-particle partitioning. Therefore, the lack of significant decay of levoglucosan in the majority of experiments in this study was interpreted as a result of the high OA mass concentrations and low temperatures. The TOMAS-VBS model demonstrated the effects of vapor wall-loss on the interpretation of levoglucosan decay in smog chamber experiments. Caution must be taken when interpreting levoglucosan decay as a function of photochemical age (or integrated OH exposure); the apparent decay rate in terms of photochemical age depends on the relative importance of vapor wall-loss and chemical degradation in addition to OA concentrations and temperature. Therefore, direct comparisons of levoglucosan decay at different temperatures, OA concentrations, OH concentrations and chambers with different vapor wall-loss rates are not valid. These

findings also highlight the importance of accounting for gas-particle-wall interactions in the investigation of the lifetime of levoglucosan or other semi-volatile marker species. This study shows that a high mass concentration of OA and low temperature extend the lifetime of the semivolatile organic markers in the atmosphere. However, as the smoke disperses, the dilution of the OA may lead to faster photochemical loss of semivolatile markers via gas-phase reactions with OH radical. It is therefore suggested to consider the OA concentrations and temperature in interpreting the lifetimes of semivolatile markers. The study also suggests that levoglucosan is a useful marker for local wintertime wood smoke/biomass burning event.

Conflicts of interest

"The authors declare no conflict of interest".

Acknowledgment

We acknowledge funding support from New York State Energy Research and Development Authority under agreement number 59809. We also thank Dr. Ellen Burkhard for helpful discussions. Dr. Pierce acknowledges funding from NSF (AGS-1559607) and NOAA (NA17OAR430001).

Appendix A. Supplementary data

Supplementary data to this article can be found online at https://doi.org/10.1016/j.atmosenv.2018.11.020.

References

Arangio, A.M., Slade, J.H., Berkemeier, T., Pöschl, U., Knopf, D. a., Shiraiwa, M., 2015. Multiphase chemical kinetics of OH radical uptake by molecular organic markers of biomass burning aerosols: humidity and temperature dependence, surface reaction, and bulk diffusion. J. Phys. Chem. https://doi.org/10.1021/jp510489z. 150225115449002.

Bergauff, M. a., Ward, T.J., Noonan, C.W., Palmer, C.P., 2009. The effect of a woodstove changeout on ambient levels of PM2.5 and chemical tracers for woodsmoke in Libby, Montana. Atmos. Environ. 43, 2938–2943. https://doi.org/10.1016/j.atmosenv.2009.02.055.

Bertrand, A., Stefenelli, G., Jen, C.N., Pieber, S.M., Bruns, E.A., Temime-Roussel, B., Slowik, J.G., Goldstein, A.H., El Haddad, I., Baltensperger, U., Prévôt, A.S.H., Wortham, H., Marchand, N., 2018a. Evolution of the chemical fingerprint of biomass burning organic aerosol during aging. Atmos. Chem. Phys. 5194, 7607–7624. https://doi.org/10.5194/acp-18-7607-2018.

Bertrand, A., Stefenelli, G., Pieber, S.M., Bruns, E.A., Temime-Roussel, B., Slowik, J.G., Wortham, H., Prévôt, A.S.H., El Haddad, I., Marchand, N., 2018b. Influence of the vapor wall loss on the degradation rate constants in chamber experiments of levoglucosan and other biomass burning markers. Atmos. Chem. Phys. 5194, 10915–10930. https://doi.org/10.5194/acp-18-10915-2018.

Bian, Q., Jathar, S.H., Kodros, J.K., Barsanti, K.C., Hatch, L.E., May, A.A., Kreidenweis, S.M., Pierce, J.R., 2017. Secondary organic aerosol formation in biomass-burning plumes: theoretical analysis of lab studies and ambient plumes. Atmos. Chem. Phys. 17, 5459–5475. https://doi.org/10.5194/acp-17-5459-2017.

Bian, Q., May, a. a., Kreidenweis, S.M., Pierce, J.R., 2015. Investigation of particle and vapor wall-loss effects on controlled wood-smoke smog-chamber experiments. Atmos. Chem. Phys. 15, 11027–11045. https://doi.org/10.5194/acp-15-11027-2015.

Carter, W.P.L., Cocker, D.R., Fitz, D.R., Malkina, I.L., Bumiller, K., Sauer, C.G., Pisano, J.T., Bufalino, C., Song, C., 2005. A new environmental chamber for evaluation of gas-phase chemical mechanisms and secondary aerosol formation. Atmos. Environ. 39, 7768–7788. https://doi.org/10.1016/j.atmosenv.2005.08.040.

Caseiro, A., Bauer, H., Schmidl, C., Pio, C.A., Puxbaum, H., 2009. Wood burning impact on PM10 in three Austrian regions. Atmos. Environ. 43, 2186–2195. https://doi.org/10.1016/j.atmosenv.2009.01.012.

Donahue, N.M., Robinson, a. L., Stanier, C.O., Pandis, S.N., 2006. Coupled partitioning, dilution, and chemical aging of semivolatile organics. Environ. Sci. Technol. 40, 2635–2643. https://doi.org/10.1021/es052297c.

Epstein, S. a., Riipinen, I., Donahue, N.M., 2010. A semiempirical correlation between enthalpy of vaporization and saturation concentration for organic aerosol. Environ. Sci. Technol. 44, 743–748. https://doi.org/10.1021/es902497z.

Gorin, C.A., Collett, J.L., Herckes, P., 2006. Wood smoke contribution to winter aerosol in Fresno, CA. J. Air Waste Manag. Assoc. 56, 1584–1590. https://doi.org/10.1080/10473289.2006.10464558.

Hawthorne, S.B., Miller, D.J., Barkley, R.M., Krieger, M.S., 1988. Identification of methoxylated phenols as candidate tracers for atmospheric wood smoke pollution. Environ. Sci. Technol. 22, 1191–1196. https://doi.org/10.1021/es00175a011.

Heal, M., 2014. The application of carbon-14 analyses to the source apportionment of atmospheric carbonaceous particulate matter: a review. Anal. Bioanal. Chem. 406, 81–98. https://doi.org/10.1007/s00216-013-7404-1.

Hennigan, C.J., Sullivan, A.P., Collett, J.L., Robinson, A.L., 2010. Levoglucosan stability in biomass burning particles exposed to hydroxyl radicals. Geophys. Res. Lett. 37, L09806. https://doi.org/10.1029/2010GL043088.

Hildebrandt, L., Donahue, N.M., Pandis, S.N., 2009. High formation of secondary organic aerosol from the photo-oxidation of toluene. Atmos. Chem. Phys. 9, 2973–2986. https://doi.org/10.5194/acp-9-2973-2009.

Huang, R.J., Zhang, Y., Bozzetti, C., Ho, K.F., Cao, J.J., Han, Y., Daellenbach, K.R., Slowik, J.G., Platt, S.M., Canonaco, F., Zotter, P., Wolf, R., Pieber, S.M., Bruns, E.A., Crippa, M., Ciarelli, G., Piazzalunga, A., Schwikowski, M., Abbaszade, G., Schnelle-Kreis, J., Zimmermann, R., An, Z., Szidat, S., Baltensperger, U., El Haddad, I., Prevot, A.S., 2014. High secondary aerosol contribution to particulate pollution during haze events in China. Nature 514, 218–222. https://doi.org/10.1038/nature13774.

Jaeckels, J.M., Bae, M.-S., Schauer, J.J., 2007. Positive matrix factorization (PMF) analysis of molecular marker measurements to quantify the sources of organic aerosols. Environ. Sci. Technol. 41, 5763–5769. https://doi.org/10.1021/es062536b.

Jathar, S.H., Gordon, T.D., Hennigan, C.J., Pye, H.O.T., Pouliot, G., Adams, P.J., Donahue, N.M., Robinson, A.L., 2014. Unspeciated organic emissions from combustion sources and their influence on the secondary organic aerosol budget in the United States. Proc. Natl. Acad. Sci. Unit. States Am. 111, 10473–10478. https://doi.org/10.1073/pnas.1323740111.

Kawamura, K., Izawa, Y., Mochida, M., Shiraiwa, T., 2012. Ice core records of biomass burning tracers (levoglucosan and dehydroabietic, vanillic and p-hydroxybenzoic acids) and total organic carbon for past 300years in the Kamchatka Peninsula, Northeast Asia. Geochem. Cosmochim. Acta 99, 317–329. https://doi.org/10.1016/j.gca.2012.08.006.

Krechmer, J.E., Pagonis, D., Ziemann, P.J., Jimenez, J.L., 2016. Quantification of gas-wall partitioning in Teflon environmental chambers using rapid bursts of low-volatility oxidized species generated in-situ. Environ. Sci. Technol. 50, 5757–5765. https://doi.org/10.1021/acs.est.6b00606.

Matsunaga, A., Ziemann, P.J., 2010. Gas-wall partitioning of organic compounds in a Teflon film chamber and potential effects on reaction product and aerosol yield measurements. Aerosol Sci. Technol. 44, 881–892. https://doi.org/10.1080/02786826.2010.501044.

May, A.A., Saleh, R., Hennigan, C.J., Donahue, N.M., Robinson, A.L., 2012. Volatility of organic molecular markers used for source apportionment analysis: measurements and implications for atmospheric lifetime. Environ. Sci. Technol. 46, 12435–12444. https://doi.org/10.1021/es302276t.

McVay, R.C., Cappa, C.D., Seinfeld, J.H., 2014. Vapor-wall deposition in chambers: theoretical considerations. Environ. Sci. Technol. 48, 10251–10258. https://doi.org/10.1021/es502170j.

Nah, T., McVay, R.C., Pierce, J.R., Seinfeld, J.H., Ng, N.L., 2017. Constraining uncertainties in particle wall-deposition correction during SOA formation in chamber experiments. Atmos. Chem. Phys. 17, 2297–2310. https://doi.org/10.5194/acp-17-2297-2017.

Ofosu, F.G., Hopke, P.K., Aboh, I.J.K., Bamford, S.A., 2013. Biomass burning contribution to ambient air particulate levels at Navrongo in the Savannah zone of Ghana. J. Air Waste Manag. Assoc. 63, 1036–1045. https://doi.org/10.1080/10962247.2013.783888.

Oros, D.R., Simoneit, B.R., 2001. Identification and emission factors of molecular tracers in organic aerosols from biomass burning Part 2. Deciduous trees. Appl. Geochemistry 16, 1545–1565. https://doi.org/10.1016/S0883-2927(01)00022-1.

Pandis, S.N., Skyllakou, K., Florou, K., Kostenidou, E., Kaltsonoudis, C., Hasa, E., Presto, A.A., 2016. Urban particulate matter pollution: a tale of five cities. Faraday Discuss 189, 277–290. https://doi.org/10.1039/C5FD00212E.

Pierce, J.R., Engelhart, G.J., Hildebrandt, L., Weitkamp, E. a., Pathak, R.K., Donahue, N.M., Robinson, a. L., Adams, P.J., Pandis, S.N., 2008. Constraining particle evolution from wall losses, coagulation, and condensation-evaporation in smog-chamber experiments: optimal estimation based on size distribution measurements. Aerosol Sci. Technol. 42, 1001–1015. https://doi.org/10.1080/02786820802389251.

Pietrogrande, M.C., Bacco, D., Ferrari, S., Kaipainen, J., Ricciardelli, I., Riekkola, M.-L., Trentini, A., Visentin, M., 2015. Characterization of atmospheric aerosols in the Po valley during the supersito campaigns — Part 3: contribution of wood combustion to wintertime atmospheric aerosols in Emilia Romagna region (Northern Italy). Atmos. Environ. 122, 291–305. https://doi.org/10.1016/j.atmosenv.2015.09.059.

Platt, S.M., El Haddad, I., Zardini, A.A., Clairotte, M., Astorga, C., Wolf, R., Slowik, J.G., Temime-Roussel, B., Marchand, N., Jezek, I., Drinovec, L., Mocnik, G., Mohler, O., Richter, R., Barmet, P., Bianchi, F., Baltensperger, U., Prevot, A.S.H., 2013. Secondary organic aerosol formation from gasoline vehicle emissions in a new mobile environmental reaction chamber. Atmos. Chem. Phys. 13, 9141–9158. https://doi.org/10.5194/acp-13-9141-2013.

Schauer, J.J., Cass, G.R., 2000. Source apportionment of wintertime gas-phase and particle-phase Air pollutants using organic compounds as tracers source apportionment of wintertime gas-phase and particle-phase Air pollutants using organic compounds as tracers. Environ. Sci. Technol. 34, 1821–1832. https://doi.org/10.1021/es981312t.

Simoneit, B.R.T., Schauer, J.J., Nolte, C.G., Oros, D.R., Elias, V.O., Fraser, M.P., Rogge, W.F., Cass, G.R., 1999. Levoglucosan, a tracer for cellulose in biomass burning and atmospheric particles. Atmos. Environ. 33, 173–182. https://doi.org/10.1016/S1352-2310(98)00145-9.

Smith, William B., Neil, Kohan, Huang Honghao, S.J., 2014. Evaluation of Wood Fuel Moisture Measurement Accuracy for Cordwood- Fired Advanced Hydronic Heaters. n.d. .

Stone, E. a., Zhou, J., Snyder, D.C., Rutter, A.P., Mieritz, M., Schauer, J.J., 2009. A

comparison of summertime secondary organic aerosol source contributions at contrasting urban locations. Environ. Sci. Technol. 43, 3448–3454. https://doi.org/10.1021/es8025209.

Szidat, S., Jenk, T.M., Synal, H.-A., Kalberer, M., Wacker, L., Hajdas, I., Kasper-Giebl, A., Baltensperger, U., 2006. Contributions of fossil fuel, biomass-burning, and biogenic emissions to carbonaceous aerosols in Zurich as traced by 14C. J. Geophys. Res. Atmos. 111https://doi.org/10.1029/2005JD006590. n/a-n/a.

Taira, M., Kanda, Y., 1990. Continuous generation system for low-concentration gaseous nitrous acid. Anal. Chem. 633, 630–633. https://doi.org/10.1021/ac00205a018.

Tkacik, D.S., Robinson, E.S., Ahern, A., Saleh, R., Stockwell, C., Veres, P., Simpson, I.J., Meinardi, S., Blake, D.R., Yokelson, R.J., Presto, A.A., Sullivan, R.C., Donahue, N.M., Robinson, A.L., 2017. A dual-chamber method for quantifying the effects of atmospheric perturbations on secondary organic aerosol formation from biomass burning emissions. J. Geophys. Res. Atmos. 122, 6043–6058. https://doi.org/10.1002/2016JD025784.

Trump, E.R., Epstein, S.A., Riipinen, I., Donahue, N.M., 2016. Wall effects in smog chamber experiments: a model study. Aerosol Sci. Technol. 50, 1180–1200. https://doi.org/10.1080/02786826.2016.1232858.

Wang, Y., Hopke, P.K., Xia, X., Rattigan, O.V., Chalupa, D.C., Utell, M.J., 2012. Source apportionment of airborne particulate matter using inorganic and organic species as tracers. Atmos. Environ. 55, 525–532. https://doi.org/10.1016/j.atmosenv.2012.03.073.

Weitkamp, E.A., Sage, A.M., Pierce, J.R., Donahue, N.M., Robinson, A.L., 2007. Organic aerosol formation from photochemical oxidation of diesel exhaust in a smog chamber. Environ. Sci. Technol. 41, 6969–6975. https://doi.org/10.1021/es070193r.

Yokelson, R.J., Griffith, D.W.T., Ward, D.E., 1996. Open-path Fourier transform infrared studies of large-scale laboratory biomass fires. J. Geophys. Res. Atmos. 101, 21067–21080. https://doi.org/10.1029/96JD01800.